Heat and Momentum Transfer in the Flow of Gases Through Packed Beds

MARVIN B. GLASER and GEORGE THODOS

The Technological Institute, Northwestern University, Evanston, Illinois

Heat and momentum transfer studies have been made for the flow of gases through fixed beds consisting of randomly packed, solid metallic particles. The experimental technique employed in these studies made possible for the first time the procurement of gas-film heat transfer data under steady state conditions and in the absence of mass transfer effects. Electric current passed through the metallic particles of the bed created within the particles a steady generation of heat, which was continuously removed by gases flowing through the bed. Several direct temperature measurements of both gases and solids within the bed made possible the direct calculation of the heat transfer coefficient for the gas film to produce the Colburn heat transfer factor j_h, which has been found to correlate with the modified Reynolds number, $Re_h = \sqrt{A_p}G/[\mu(1 - \epsilon)\varphi]$. The shape factor φ was established in these studies for cubes and cylinders and was found to be identical to their respective sphericities.

Pressure-drop measurements produced a friction factor f_k of the Blake type, which yielded separate curves for each shape when correlated with the modified Reynolds number Re_m. No simple relationship was found to exist between the heat transfer and friction factors. A single correlation of the pressure-drop data was obtained for the modulus $f_k\varphi^n$ when correlated with a Reynolds number of the type $Re_m = \sqrt{A_p}G/[\mu(1 - \epsilon)]$. The exponent n varies with the particle shape.

Experimental runs have been carried out for 3/16, 1/4, 5/16-in. spheres, 1/4 and 3/8-in. cubes, and regular cylinders using hydrogen and carbon dioxide to extend the range of molecular weights beyond that of air, used for the majority of these runs. A particle-size, column-diameter effect was found to exist for both heat and momentum transfer. This effect becomes significant in the low Reynolds region.

Investigations dealing with the flow of heat between granular solids and flowing gases have been associated with simultaneous mass transfer or have been involved with unsteady state conditions (*1*, *2*, *3*, *9*, *11* to *16*). The heat transfer correlations produced from mass transfer studies involved the vaporization of a liquid from a solid surface, and as a result the heat transfer data were obtained indirectly. Thus Gamson et al. (*9*) and Taecker and Hougen (*15*) vaporized water from porous catalyst carriers and, by assuming adiabatic conditions, were able to establish the gas and particle temperatures with a humidity chart. Satterfield, Resnick, and Wentworth (*13*) decomposed hydrogen peroxide in the presence of metallic spheres to obtain simultaneous mass and heat transfer data. Heat transfer coefficients for the gas film were produced from measured sphere temperatures, and the calculated heat generated on the catalyst surface was assumed to transfer completely to the flowing gas.

Early attempts to establish independent heat transfer mechanisms associated in the flow of gases through granular particles were of the unsteady state type as described by Schumann (*14*) and Furnas (*8*). The interpretation of these results in terms of an average heat transfer coefficient was difficult because of the prevailing transient conditions and mathematical complexity of the problems.

The correlation of pressure-drop data for the flow of gases through porous media, which first considered the inclusion of the void volume effect, was proposed in 1922 by Blake (*4*) from dimensional-analysis considerations. Further developments resolved the total momentum transfer encountered into kinetic- and viscous-energy contributions. Using these concepts, Ergun (*7*) presented the pressure-drop expression

$$\frac{g_c \Delta P}{L} \frac{D_p}{Gu} \frac{\epsilon^3}{1 - \epsilon} = f_k \qquad (1)$$

where f_k is a function of the modified Reynolds number, $Re' = D_pG/[\mu(1 - \epsilon)]$. In Equation (1) f_k represents the ratio of total-energy losses to kinetic-energy losses. A review of the literature points to the fact that this pressure-drop relation produces a dependable correlation with experimental data.

Colburn (*6*) derived and experimentally verified a similarity between heat, mass, and momentum transfer for the flow of fluids through circular conduits; however, the possible existence of such an analogy for the flow of fluids through granular beds has been highly controversial.

The present investigation has been initiated primarily to establish heat transfer coefficients for gases flowing through a fixed bed of randomly packed granular particles in the absence of mass transfer effects and under steady state conditions. As a secondary consequence, the simultaneous pressure-drop information would permit a reevaluation of the possibility of the existence of an analogy between heat and momentum transfer.

EXPERIMENTAL EQUIPMENT AND PROCEDURE

The experimental unit was designed to produce uniform heat generation within a granular bed consisting of metallic particles for which heat removal was accomplished by the flow of gases. Radial heat transfer was eliminated in order to ensure accuracy in the measurement of heat generated. Simultaneous pressure-drop measurements were made with an inclined-draft gauge.

A schematic diagram of the equipment is presented in Figure 1, which includes the column containing the packed bed. This column with its auxiliaries is shown in Figure 2. Compressed air from the building supply was regulated and passed through a filter for the removal of entrained oil and water prior to metering through Fischer-Porter flowmeters connected in parallel. In a similar fashion carbon dioxide and hydrogen furnished from high-pressure gas cylinders were pressure regulated and passed through the flowmeters. After being metered, the gas was introduced into the column to remove from the fixed bed the heat which was generated by the passage of electric current through the metallic particles of the bed. The electric current for heating the bed was provided from a specially designed

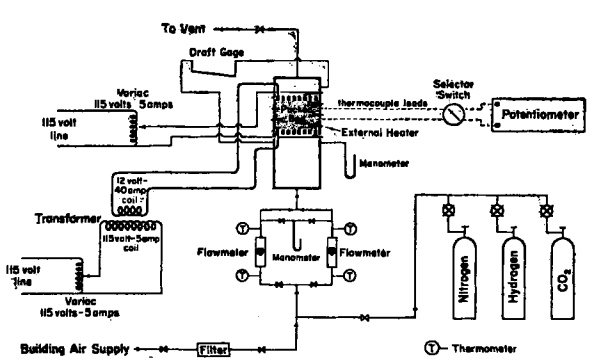

Fig. 1. Schematic diagram of experimental unit.

Marvin B. Glaser is at present with the Esso Research and Engineering Company, Linden, New Jersey.

high-amperage, low-voltage transformer, which has a primary rating of 115 volts, 5 amp. and a secondary rating of 12 volts, 40 amp. Current to the transformer was controlled with a conventional 115-volt, 5-amp. variac. The heated gases after leaving the column were vented to the atmosphere.

Figure 2 presents the details of the vertical column which was prepared from a transite pipe having an inside diameter of 2 in. Transite was selected because of its excellent electrical and thermal insulating properties and its machineability. The column consisted of three distinct sections. The bottom section, 9 in. in length, contained a 6-in. section packed with ball bearings, which served to calm and distribute the gas flow evenly into the heat transfer section. The lower column section also contained pressure taps and one of the heavy copper leads which contacted the heat transfer section. Similarly, pressure taps and another heavy copper lead were contained in the upper column section, which was 3 in. long. The middle section, 4 in. long, contained the packed bed of metallic particles, supported between perforated stainless steel plates $\frac{1}{16}$ in. thick, which served as the electrodes of the bed. These three separate component sections were assembled by superimposition. When pressure was applied between the calming section and the upper section, the packing in the middle section became fixed. The necessary pressure was supplied to the bed by four steel compression rods, which spanned the full length of the column between two steel flanges.

When the column was assembled, the two copper leads contacted the perforated-plate electrodes to permit the flow of electric current through the bed. Thus the resistance of the metallic bed was responsible for the generation of heat within the solid particles. The application of proper pressures on the compression rods permitted the even distribution of electric current through the bed in order to ensure uniform heating. Through these means the total bed resistance could be varied from 1 to 5 ohms. It is probable that a large portion of the total heat was generated at the points of particle contact; however, a uniform particle temperature was obtained because of the high thermal conductivities of the metals used and the multiplicity of contact points per particle.

External heat was supplied to the heat transfer section in order to eliminate radial temperature gradients within the bed. This was accomplished by means of a $\frac{1}{8}$-in. nichrome strip heater, which was wrapped around the heat transfer section of the column. Two iron-constantan thermocouples were embedded in the heat transfer wall and spaced on a common radius so that one thermocouple was located near the inside radius and the other was near the outside. Adiabatic conditions were realized when these two thermocouples indicated the same temperature.

Iron-constantan thermocouples of 24 B and S gauge thickness and covered with glass and asbestos insulation were used to measure particle and gas temperatures within the bed. A total of twelve thermocouples were located in each bed and were connected to a Brown single-point electronic potentiometer which had a 4.5-sec. full-dial response. This potentiometer was connected to three multipoint thermocouple switches. The thermocouple leads were brought into the bed through small holes drilled in the column wall. After the lead wires had been inserted, the holes were sealed with litharge. Some thermocouples were permanently attached to the particle surfaces by drilling a small hole through a major diameter and inserting the thermocouple wire through this hole until the couple junction reached a point just below the opposite surface, whereupon it was fastened in place with a drop of solder. Generally, two or three thermocouples were placed in a cross-sectional area of the bed at different radial distances in order to check the uniformity of heat generation.

The rest of the thermocouples were placed between the interstices of the bed and forced against the surface of the solid particles. These unfastened thermocouples were then positioned in the void spaces of the bed by means of the following sensitive procedure to ensure proper placement. After the entire bed was in place, electric current was passed through it for the generation of heat. Gas was then allowed to flow through the bed. When equilibrium conditions had been attained, the temperatures indicated by all thermocouples in any given cross section were found to record approximately the same temperatures, varying at most by 0.5°F. The unattached thermocouples were moved gently by applying a slight pull on the lead wires until their indicated temperature suddenly dropped. At this position the thermocouple junction was assumed to be surrounded completely by gas, the temperature of which could be directly measured. The thermocouple was then frozen in this position with the application of litharge to the lead-wire wall-entry hole. The radial position of this thermocouple was indicated from designated markings on the lead wires.

This procedure enabled the procurement of solid and gas temperatures for different cross sections of the bed and thus established the longitudinal temperature profiles for the entire bed length. These temperature profiles made possible the calculation of point heat transfer coefficients, thus eliminating the influence of end effects caused by the perforated-plate electrodes.

Three types of metallic packings, consisting of spheres, cubes, and regular cylinders, were investigated. The properties of these packings and the various beds used are presented in Table 1. All spheres were commercial ball bearings ground to rigid specifications. The cubes and cylinders were prepared by cutting steel rods into the desired size particles. Tolerances for the cubes and cylinders were limited to ±0.003 in.

Seven randomly packed beds were investigated with reference to shape, size, and void volume. The void volume of each bed was determined in *situ* by placing the required number of particles to fill the heat transfer section of the column included between the two electrodes. The total solid volume of the particles was established from the number and the calculated volume of the particles. Each bed was prepared by dropping particles individually into the column. When the desired level had been reached, particles containing fixed thermocouples were carefully positioned before the further addition of packing. Air, hydrogen,

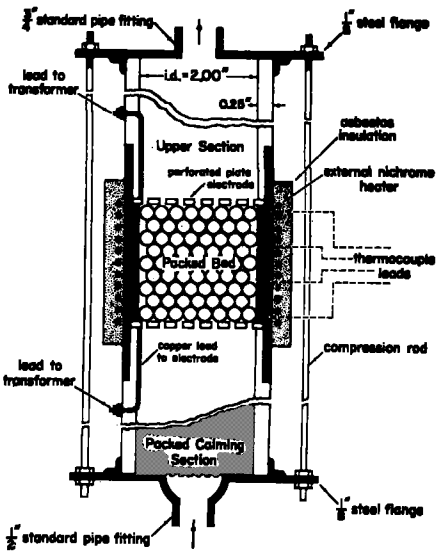

Fig. 2. Detailed sketch of transite column.

and carbon dioxide were the gases employed with each bed and were used in order to cover the range of molecular weights for the common gases.

A number of preliminary tests were performed on each bed in order to determine the uniformity of internal heat generation. First, current was supplied to the bed with no gas flow, and the temperatures of all particles equipped with thermocouples were examined after a short heating period and were found to be constant within 0.5°F. A

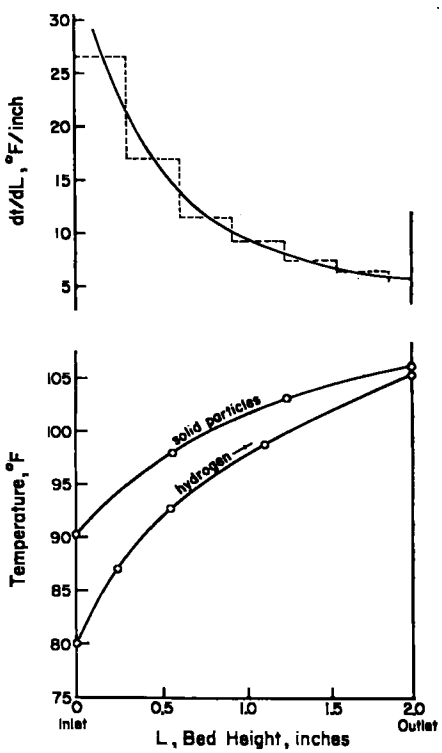

Fig. 3. Longitudinal temperature profiles for the flow of hydrogen through packed spheres and resulting gas temperature gradient (run 63-1/4-in. spheres).

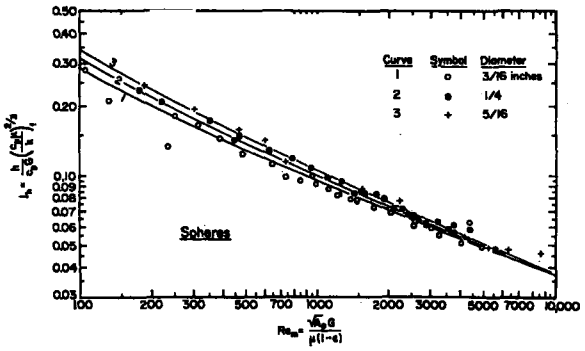

Fig. 4. Heat transfer factors for packed beds of spheres.

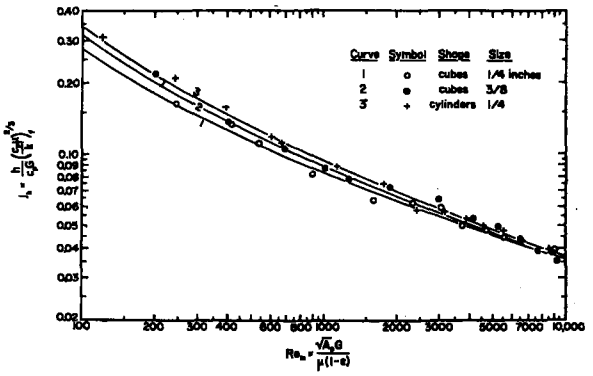

Fig. 5. Heat transfer factors for packed beds of cubes and cylinders.

total time of approximately 10 sec. was required to obtain all these readings. The passage of the electric current through the bed did not influence the performance of the thermocouples, as the galvanometer of the potentiometer does not respond sufficiently to the 60-cycle current of the magnitude used to heat the bed. Air was then passed through the bed at a constant rate, and the temperatures of the particles in any cross section were found to be essentially constant; for nearly all runs they averaged within 1° to 2°F. of each other. Therefore, an average of the solid temperatures in a given cross section was used to represent the temperature of the particles in that cross section.

Steady state conditions were realized for each run. One hundred and eighteen runs, which included simultaneous heat and momentum transfer, were made, and 65 additional runs were conducted for the purpose of securing a more extensive background for pressure-drop measurements (*10*). In order to minimize radiation effects, the temperature differential between the inlet and outlet gas was limited to 50°F., and the maximum particle temperature was not allowed to exceed 150°F. For the hydrogen runs the entire system was first purged with nitrogen in order to eliminate any hazard of an air-hydrogen explosion, which could be caused by an electric spark.

INTERPRETATION OF HEAT TRANSFER DATA

The method used to calculate the local heat transfer coefficient for the gas film involved the consideration of a differential height of bed dL. Since heat is being generated within the particles and is completely transferred to the flowing gas at the steady rate q, a heat balance over the differential segment shows that

$$q = wc_p\,dt = h_g a(S\,dL)(T - t) \qquad (2)$$

The local heat transfer coefficient h_g is obtained by rearranging Equation (2) into the form

$$h_g = \frac{c_p G}{a(T - t)}\left(\frac{dt}{dL}\right) \qquad (3)$$

A typical plot of longitudinal gas- and solid-temperature profiles is presented in Figure 3 for run 63. A graphical differentiation of the gas-temperature profile by means of the chord-area method produced the gas-temperature gradient dt/dL, presented in Figure 3. For a fixed point within the bed the values $T - t$ and dt/dL were obtained directly to produce the local heat transfer coefficient h_g from Equation (3). In general, coefficients were evaluated at four equidistant points ranging from ¼ to 1¼ in. from the bed entrance. A variation of approximately ±5% was noted for the calculated local heat transfer coefficient for each bed. An arithmetic average of the local coefficients was used to obtain an average coefficient for the entire bed.

Heat transfer factors defined by Colburn (*5*) as

$$j_h = \frac{h}{c_p G}\left(\frac{c_p\mu}{k}\right)_f^{2/3} \qquad (4)$$

were calculated from the average coefficients and average film properties. A summary of these calculated values and properties is presented in Table 2 for the 5/16-in. spheres only. The complete listing of the results presented in Table 2 for all the seven different beds of Table 1 are available elsewhere (*10*). The calculated values of j_h are plotted in Figures 4 and 5 against a Reynolds number of the type $Re_m = \sqrt{A_p}G/[\mu(1 - \epsilon)]$, where $\sqrt{A_p}$ expresses a linear dimension characteristic of the particle.

An inspection of Figures 4 and 5 shows that the data for each individual bed produce good correlations; however, these correlations are distinct within themselves and depend on particle shape and size. Lack of a generalized correlation for the three sizes of spheres is apparent in Figure 4, in which the effect of particle size is found to be most significant in the region of low Reynolds number. Similar behavior is shown in Figure 5 for two sizes of cubes. It is also apparent from Figures 4 and 5 that no correlation exists between spheres, cubes, and cylinders of the same size.

The lack of a single correlation for different sizes of the same type of packing is attributed to a ratio of particle size to column diameter. These ratios, expressed as D_p/D_r, become for the three sizes of spheres 0.10, 0.133, 0.167 and extend beyond the recommended limit for packed columns of 0.125.

The absence of a single correlation for different particle shapes is due to the unavailability of a fraction of the entire particle surface area which results from particle-area contacts. For spheres, particle contacts are point contacts; whereas for shapes such as cubes and cylinders, the contacts may involve significant areas. In order to take into account the actual surface involved in the transfer of heat and mass, the shape factor φ, representing the fraction of the total participating surface, has been developed to introduce φ into the modified Reynolds number as follows. By definition

$$Re = \frac{G}{(a\varphi)\mu} \qquad (4)$$

where the product $a\varphi$ represents the participating transfer area. For spheres, cubes, and regular cylinders, it can be shown that

$$a = \frac{6}{D_p}(1 - \epsilon) \qquad (5)$$

where D_p represents a characteristic particle dimension. Eliminating a from Equation (4) yields the Reynolds number

$$Re = \frac{D_p G}{6(1 - \epsilon)\varphi\mu} \qquad (6)$$

Furthermore, the surface area of a particle A_p can be expressed in terms of D_p as $A_p = KD_p^2$ where K is a constant depending on the particle geometry. When the quantity $D_p = \sqrt{A_p/K}$ is substituted, a Reynolds number can be expressed in terms of these variables as

$$Re_h = \frac{\sqrt{A_p}G}{\mu(1 - \epsilon)\varphi} \qquad (7)$$

For spheres the shape factor φ has been

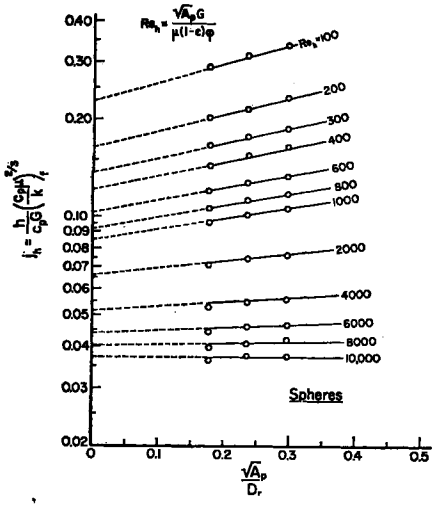

Fig. 6. Relationships of heat transfer factor with equivalent particle-size, column-diameter ratio for spheres.

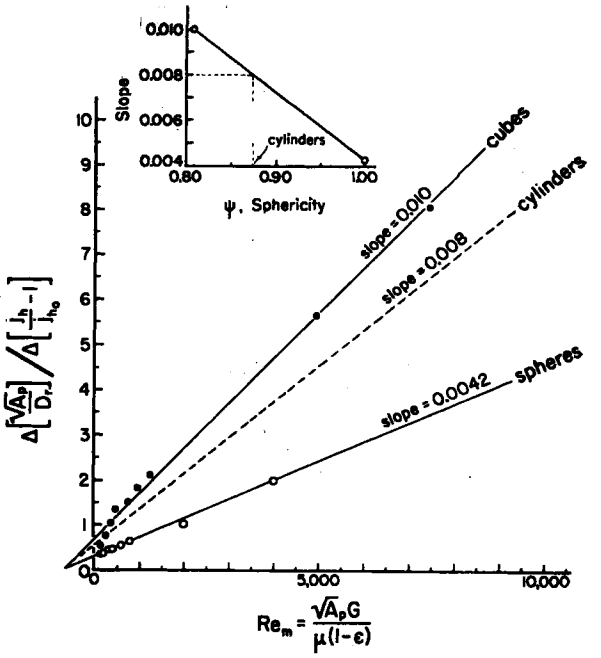

Fig. 7. Relationship of the quantity

$$\Delta\left[\frac{\sqrt{A_p}}{D_r}\right] \Big/ \Delta\left[\frac{j_h}{j_{h_o}} - 1\right]$$

with the modified Reynolds number, Re_m, for spheres and cubes.

taken as one, and for other particles this factor becomes less than unity.

A correlation of particle size and column diameter expressed as $\sqrt{A_p}/D_r$ was first established for spheres and involved plotting the values of j_h presented in Figure 4 against the ratio $\sqrt{A_p}/D_r$ for parameters of constant Reynolds number, as shown in Figure 6. Extrapolations of the resulting plots to $\sqrt{A_p}/D_r = 0$ produced heat transfer factors which have been designated as j_{h_o} and correspond to the case where the particle size is negligible in relation to column diameter. It is to be expected that for large values of $\sqrt{A_p}/D_r$ the curves of Figure 6 will approach a limiting j_h value. A relation between j_h/j_{h_o} and $\sqrt{A_p}/D_r$ in terms of the Reynolds number Re_h has been found to apply for spheres in the interval $100 < Re_h < 9{,}200$, which can be expressed empirically as

$$\frac{j_h}{j_{h_o}} = 1 + \frac{\sqrt{A_p}}{D_r} \log \frac{4984}{Re_h^{0.933}} \qquad (8)$$

where

$$j_{h_o} = \frac{0.535}{Re_h^{0.30} - 1.6} \qquad (9)$$

For $Re_h > 9{,}200$ the ratio j_h/j_{h_o} is unity and thus is consistent with the experimental results.

A similar procedure was applied to the data of the two sizes of cubes having edges of ¼ and ⅜ in. Before a shape factor for cubes was established, values of j_{h_o} were determined by extrapolating the curves resulting from plots of j_h vs. $\sqrt{A_p}/D_r$ for parameters of $\sqrt{A_p}G/[\mu(1-\epsilon)]$. The proper shape factor for cubes was determined through a trial-and-error procedure which consisted of applying assumed values of φ in Equation (7) until the resulting curve of j_{h_o} vs. Re_h for cubes became coincidental with the previously determined curve for spheres. For cubes the shape factor was found to be $\varphi = 0.81$. In addition, the relationship between j_h and j_{h_o} for cubes can be expressed conveniently as

$$\frac{j_h}{j_{h_o}} = 1 + \frac{\sqrt{A_p}}{D_r} \frac{23.1}{Re_h^{0.626}} \qquad (10)$$

where j_{h_o} is defined by Equation (9) and applies in the interval $100 < Re_h < 9{,}200$. It is noteworthy that, even though the variations of j_h with Re_h for cubes and spheres are different, the variation of j_{h_o} with Re_h is identical.

The extensive investigation of spheres and cubes was used as a basis to establish the variation of j_h with $\sqrt{A_p}/D_r$ for the only available heat transfer data for ¼-in. regular cylinders. Since these data were limited to one size of cylinders, values of j_{h_o} could not be obtained by

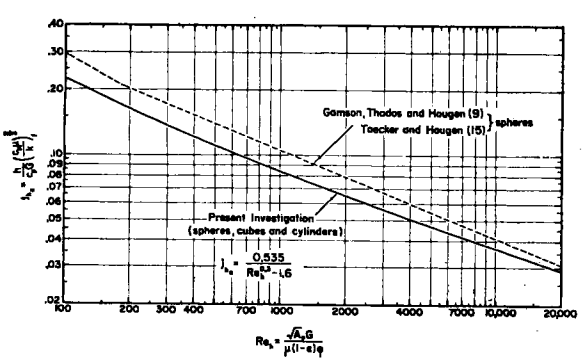

Fig. 8. Heat transfer factors for packed beds.

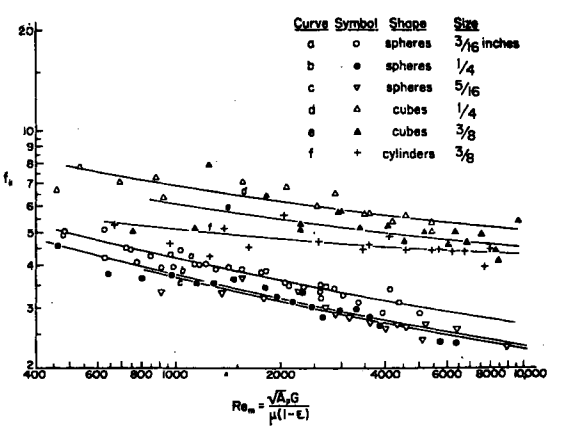

Fig. 9. Friction factors for packed beds of spheres, cubes and cylinders.

the method described for spheres and cubes, as at least two experimental values of $\sqrt{A_p}/D_r$ are required. To establish this relation for cylinders, values of $(j_h/j_{h_0}) - 1$ were plotted against $\sqrt{A_p}/D_r$ for spheres and cubes with parameters of the Reynolds number Re_m. This Reynolds number has been used here in order to establish j_{h_0} independently of φ. The resulting straight lines converged at the origin and produced reciprocal slopes, which were correlated against the Reynolds number Re_m, as shown in Figure 7. It was assumed that the slopes of the straight lines of Figure 7 for spheres and cubes were directly related to their respective sphericities (ψ) of 1.00 and 0.806 as shown in Figure 7. Sphericity represents the ratio of the surface area of a sphere having the same volume as a particle to the surface area of the particle. On the assumption that this relation also applies to cylinders of $\psi = 0.873$, a slope of 0.008 was obtained for regular cylinders to produce the dotted line of Figure 7. Direct readings for cylinders produced the quantity $\Delta[\sqrt{A_p}/D_r]/\Delta[(j_h/j_{h_0}) - 1]$, which was associated with the experimental values of j_h and $\sqrt{A_p}/D_r$ to define j_{h_0} for cylinders as follows:

$$\frac{j_h}{j_{h_0}} = 1 + \frac{\sqrt{A_p}}{D_r}\frac{10.78}{Re_h^{0.384}} \qquad (11)$$

In the same procedure as that used for cubes, a shape factor of $\varphi = 0.88$ was necessary to superimpose the data of cylinders on those of the spheres and cubes. The resulting plot of j_{h_0} vs. Re_h for this investigation, involving spheres, cubes, and cylinders, is presented in Figure 8 and is compared with the converted data of Gamson et al. (*9*) and Taecker and Hougen (*15*). These expressions produce for packed beds results that have been found to be consistent with actual practice involving the regeneration of catalysts used in hydroforming work.

In these heat transfer studies the shape factors φ for spheres, cubes, and cylinders were calculated independently. A comparison of these shape factors with particle sphericities presents a strong indication that the shape factors used in these studies and particle sphericities may be interchangeable for packed beds. A summary of the experimentally determined shape factors and calculated particle sphericities follows:

Particle shape	Shape factor φ	Sphericity ψ
Spheres	1.0	1.0
Cylinders	0.88	0.873
Cubes	0.81	0.806

Further work with irregularly shaped packings, such as partition rings, Raschig rings, and Berl saddles, is necessary before any definite conclusion can be reached regarding a relationship between the shape factor φ and ψ, the sphericity.

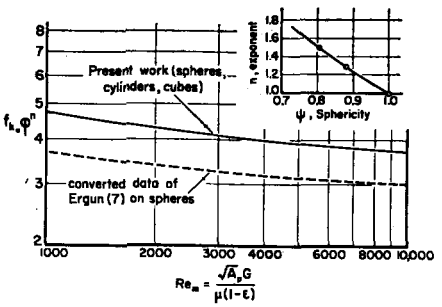

Fig. 10. Correlation of friction modulus and Reynolds number for packed beds.

INTERPRETATION OF PRESSURE-DROP DATA

Pressure-drop data are presented for 5/16-in. spheres in Table 2, and the complete data for all the spheres, cubes, and cylinders are presented elsewhere (*10*). The pressure drop due to the perforated electrodes has been subtracted from the total pressure loss to produce the pressure drops across the bed given in Table 2. Friction factors f_k have been calculated with a modification of Equation (1) in order to be consistent with the characterizing dimension of the packing $\sqrt{A_p}$. Thus Equation (1) becomes

$$\frac{g_c\Delta P}{L}\frac{\sqrt{A_p}}{Gu}\frac{\epsilon^3}{1-\epsilon} = f_k \qquad (12)$$

A summary of the calculated values of f_k appears in Table 2 for 5/16-in. spheres. All the values of f_k are presented as a function of the Reynolds number Re_m in Figure 9.

Figure 9 shows the existence of separate relationships for each particle shape and size. The friction factor f_k increases with decreasing particle size, which is opposite to the behavior of the heat transfer

TABLE 1. PROPERTIES OF PACKED BEDS

(Column diameter = 1⅞ in.; bed height = 2.0 in.)

No.	Particle shape	Type of metal	Particle size, in.	Total number of particles in bed	a, sq. ft./cu. ft.	ϵ, fractional void volume	$\frac{\sqrt{A_p}}{D_r}$
1*	Sphere	Monel	3/16	935	217	0.436	0.177
2	Sphere	Brass	¼	392	164.5	0.429	0.236
3	Sphere	Brass	5/16	190	126	0.453	0.296
4	Cube	Steel	⅜ (edge)	56	102	0.469	0.490
5	Cube	Steel	¼ (edge)	207	168.5	0.417	0.325
6†	Regular cylinder	Steel	¼	234	151	0.477	0.289
7‡	Regular cylinder	Steel	⅜	70	100	0.478	0.433

*Bed height of 2 1/16 in.
†Heat transfer studies only.
‡Momentum transfer studies only.

TABLE 2. HEAT AND MOMENTUM TRANSFER RESULTS FOR 5/16-in. SPHERES

Run	G, lb./(hr.)(sq. ft.)	ΔP, in. of water*	h, B.t.u./(hr.)(sq. ft.)(°F.)	$\frac{h}{C_pG}$	$\frac{\sqrt{A_p}G}{(1-\epsilon)}$	j_h	f_k
Air: $(c_p\mu/k)^{2/3} = 0.796$							
65	396	0.126	13.47	0.1415	741	0.113	5.77
66	816	0.338	21.30	0.1087	1562	0.0865	3.70
67	1,165	0.620	27.27	0.0974	2250	0.0775	3.39
68	1,511	0.930	28.38	0.0780	2900	0.0622	2.90
69	1,880	1.30	31.80	0.0704	3620	0.0562	2.73
70	2,240	1.81	36.32	0.0676	4320	0.0538	2.68
71	2,760	2.77	40.73	0.0615	5330	0.0490	2.72
Hydrogen: $(c_p\mu/k)^{2/3} = 0.800$							
72	122.8	—	82.48	0.1949	478	0.1561	
73	79.8	—	65.62	0.2395	309	0.1915	
74	49.1	—	51.54	0.3050	190	0.2440	
75	159.5	0.246	97.47	0.1765	616	0.1405	5.05
Carbon dioxide: $(c_p\mu/k)^{2/3} = 0.762$							
76	3,640	2.66	44.60	0.0613	8820	0.0467	2.33
77	2,660	1.82	33.43	0.0630	6450	0.0480	2.62
78	1,740	0.915	24.93	0.0717	4230	0.0547	3.40

*The pressure drop due to the perforated-plate electrodes has been subtracted from the total pressure drop to produce the values presented in this table.

factor j_h with particle size. The reason momentum and heat transfer are not directly related in packed beds is that momentum transfer involves surfaces, corners, and edges, whereas heat transfer is restricted to surface areas. The effect of reactor diameter is due to a difference in gas velocities at wall surfaces and through packing not in contact with the wall. The geometry of contact is different at the wall surface from that between particles in the bed, which are removed from the wall. Hence, the correlations for both momentum transfer and for heat transfer are altered in opposite directions, as shown by this investigation.

Since the friction-factor relationships of Figure 9 are nearly horizontal, the use of the shape factor φ in the Reynolds number Re_h did not prove adequate for correlating these data. In general, the pressure-drop data for each individual shape and size did not correlate as well as the corresponding heat transfer data. The lack of a good correlation for momentum transfer can be attributed to the thin beds employed, under which conditions the entrance and exit effects may be significant. Furthermore, for low flow rates the resulting pressure losses were very small and hence were difficult to measure. Consequently, the correlation of pressure drop was limited to the region $1{,}000 < Re_m < 10{,}000$.

The friction-factor data for spheres, cubes, and cylinders were analyzed in a manner similar to that used for the heat-transfer-factor correlation in order to establish the particle-size, column-diameter effect on f_k. Values of f_{k_o} representing friction factors at $(\sqrt{A_p}/D_r) \rightarrow 0$ were obtained for spheres, cubes, and cylinders to produce separate correlations for each shape when plotted against the Reynolds number Re_m. A single correlation for these shapes resulted when the shape factor φ was directly associated with the friction factor f_{k_o} in the dimensionless modulus $f_{k_o}\varphi^n$, where n is an exponent which can be related to sphericity. The value of n is unity for spheres, and for cylinders and cubes it was established by trial and error to be 1.29 and 1.50, respectively. A plot of the friction modulus $f_{k_o}\varphi^n$ vs. the Reynolds number Re_m for the range included between $Re_m = 1{,}000$ to 10,000 is presented in Figure 10 along with the relationship for n and the sphericity ψ. This correlation is compared with the converted results of Ergun (7) for spheres, which also appear in Figure 10. For the range $1{,}000 < Re_m < 10{,}000$, the friction modulus can be expressed empirically as

$$f_{k_o}\varphi^n = \frac{2.89}{Re_m^{0.05} - 0.81} \qquad (13)$$

The relationships of the friction factor f_k and the friction factor f_{k_o} for the limiting case when $(\sqrt{A_p}/D_r) \rightarrow 0$ can be expressed empirically for spheres, cubes, and cylinders as follows:

spheres

$$\frac{f_{k_o}}{f_k} = 1 + \frac{\sqrt{A_p}}{D_r} \log \frac{Re_m^{1.25}}{8.22} \qquad (14)$$

cubes

$$\frac{f_{k_o}}{f_k} = 1 + \frac{\sqrt{A_p}}{D_r} \frac{Re_m^{0.104}}{3.25} \qquad (15)$$

cylinders

$$\frac{f_{k_o}}{f_k} = 1 + \frac{\sqrt{A_p}}{D_r} \frac{Re_m^{0.193}}{4.91} \qquad (16)$$

COMPARISON OF HEAT AND MOMENTUM TRANSFER FACTORS

In order to investigate the possible existence of an analogy between the heat transfer factor, j_{h_o} and the momentum transfer factor f_{k_o} comparisons of these moduli were limited to the simple geometry existing for spheres which have values of $\varphi = 1.0$ and $n = 1.0$. The ratio of j_{h_o}/f_{k_o} was found to decrease steadily from 0.165 at $Re_m = 1{,}000$ to 0.100 at $Re_m = 10{,}000$. The existence of a direct relationship between these factors remains to be substantiated experimentally and is highly unlikely as long as the total momentum transfer cannot be resolved into the contributions due to skin friction and the impediments to flow created by edge and corner effects.

ACKNOWLEDGMENT

The authors wish to acknowledge the assistance of D. F. Mason and B. J. Sollami, who contributed to the experimental design of the equipment.

NOTATION

a = surface of particles per unit volume of bed, sq. ft./cu. ft.
A_p = surface area of individual particle, sq. ft.
c_p = heat capacity at constant pressure, B.t.u./(lb.)(°F.)
D_p = equivalent particle diameter, ft.
D_r = column diameter, ft.
f_k = friction factor for packed beds, $(g_c \Delta P/L)(\sqrt{A_p}/Gu)(\epsilon^3/1 - \epsilon)$
f_{k_o} = friction factor for $(\sqrt{A_p}/D_r) \rightarrow 0$
g_c = gravitational constant, 32.2 (lb.-mass)(ft.)/(lb.-force)(sec.)^2
G = superficial mass velocity, (lb.)/(hr.)(sq. ft.)
h = heat transfer coefficient, B.t.u./(hr.)(sq. ft.)(°F.)
h_g = gas-film heat transfer coefficient, B.t.u./(hr.)(sq. ft.)(°F.)
j_h = heat transfer factor, dimensionless
j_{h_o} = heat transfer factor for $(\sqrt{A_p}/D_r \rightarrow 0$
k = thermal conductivity, B.t.u./(hr.)(ft.)(°F.)
K = constant
L = bed height, ft.
n = exponent
P = pressure, lb.-force/sq. ft.
q = rate of heat transfer, B.t.u./hr.
Re' = modified Reynolds number, $D_pG/[\mu(1 - \epsilon)]$
Re_h = modified Reynolds number for heat transfer, $\sqrt{A_p}G/[\mu(1 - \epsilon)\varphi]$
Re_m = modified Reynolds number for momentum transfer, $\sqrt{A_p}G/[\mu(1 - \epsilon)]$
S = column cross-sectional area, sq. ft.
t = temperature of flowing gas, °F.
T = temperature of particle, °F.
u = average linear fluid velocity, ft./sec.
w = mass flow rate, lb./hr.

Greek Letters

ϵ = fractional void volume, dimensionless
μ = absolute viscosity, lb./(hr.)(ft.)
ρ = average fluid density, lb./cu. ft.
φ = particle shape factor, fraction of total participating surface of particle, dimensionless
ψ = particle sphericity, $\frac{\text{surface area of sphere having same volume as particle}}{\text{surface area of particle}}$, dimensionless

LITERATURE CITED

1. Amundson, N. R., *Ind. Eng. Chem.*, **48**, 26 (1956).
2. Anzelius, A., *Z. angew. Math. u. Mech.*, **6**, 291 (1926).
3. Arthur, J. R., and J. W. Linett, *J. Chem. Soc.*, Part 1, 416 (1947).
4. Blake, F. E., *Trans. Am. Inst. Chem. Engrs.*, **14**, 415 (1922).
5. Colburn, A. P., *Ind. Eng. Chem.*, **23**, 910 (1931).
6. ———, *Trans. Am. Inst. Chem. Engrs.*, **29**, 174 (1933).
7. Ergun, Sabri, *Chem. Eng. Progr.*, **48**, 89 (1952).
8. Furnas, C. C., *Ind. Eng. Chem.*, **22**, 721 (1930).
9. Gamson, B. W., George Thodos, and O. A. Hougen, *Trans. Am. Inst. Chem. Engrs.*, **39**, 1 (1943).
10. Glaser, M. B., Ph.D. thesis, Northwestern Univ., Evanston, Ill. (August, 1956).
11. Katz, S., and A. M. Reiser, *J. Math. Physics*, **33**, 256 (1954).
12. Löf, G. O. G., and R. W. Hawley, *Ind. Eng. Chem.*, **40**, 1061 (1948).
13. Satterfield, C. N., Hyman Resnick, and R. L. Wentworth, *Chem. Eng. Progr.*, **50**, 460 (1954).
14. Schumann, T. E. W., *J. Franklin Inst.*, **208**, 405 (1929).
15. Taecker, R. G., and O. A. Hougen, *Chem. Eng. Progr.*, **45**, 188 (1949).
16. Wilhelm, R. H., W. C. Johnson, and F. S. Acton, *Ind. Eng. Chem.*, **35**, 561 (1943).

Manuscript submitted October 3, 1956; revision received August 8, 1957; paper accepted September 4, 1957.